



Optimizing microdisplay requirements for pancake VR applications

En-Lin Hsiang, SID student member | Zhiyong Yang, SID student member  | Shin-Tson Wu, SID Fellow 

College of Optics and Photonics,
University of Central Florida, Orlando,
Florida, USA

Correspondence

Shin-Tson Wu, College of Optics and
Photonics, University of Central Florida,
Orlando, FL 32816, USA.

Email: swu@creol.ucf.edu

Funding information

Nichia Corporation

Abstract

Virtual reality (VR) devices use imaging optics to magnify the microdisplay images for providing an immersive viewing experience. A microdisplay is preferred to have high-resolution density and high dynamic range to meet the demanding requirements of human vision system (HVS), for example, visual acuity >60 pixels per degree and grayscale depth >10 bits. However, increasing resolution density and dynamic range often lead to a reduced optical efficiency and sophisticated fabrication process of the microdisplay panels. In this paper, we systematically analyze the image degradation mechanisms of VR devices caused by both imaging optics and microdisplay and find that the image degradation caused by imaging optics significantly unleash the requirements of microdisplay, such as contrast ratio, number of local dimming zones, and resolution density. For example, aberrations of the imaging optics reduce the resolution density requirement of the microdisplay, and stray light of the imaging optics relieves the contrast ratio requirement of the microdisplay. These results help prevent excessive design of microdisplay, for example, mini-light-emitting diode (LED) backlit liquid-crystal displays (LCDs), organic LEDs, or micro-LEDs, in a pancake lens-based VR headset.

KEYWORDS

high-resolution density, microdisplays, pancake lens, virtual reality displays

1 | INTRODUCTION

With the rapid development of Metaverse, there is an urgent need to optimize the microdisplays for virtual reality (VR) devices with vibrant three-dimensional (3D) virtual images.^{1–3} In a VR device, the image from microdisplays is first magnified by the imaging optics and then received by the human visual system. In the past, the requirements of a microdisplay are designed based on the visual acuity and dynamic range of human vision system (HVS). The magnified image after imaging optics should support visual acuity of 60 pixels per degree (ppd) and sufficient dynamic range. Therefore, microdisplays

with high-resolution density and high dynamic range (HDR) are required.

From the perspective of high-resolution density, according to the focal length of the imaging optics (40 mm) and the target visual acuity (60 ppd), the required resolution density for the microdisplay is calculated to be about 2200 ppi.⁴ Moreover, the required resolution density is inversely proportional to the focal length of the imaging optics. Therefore, an advanced catadioptric imaging optics, known as pancake lens, helps shorten the focal length (<30 mm) to obtain a more compact form factor, but it requires a higher resolution density microdisplay (>3000 ppi). The major challenge of a

high-resolution density liquid-crystal display (LCD) is its relatively low optical efficiency⁵ and a white organic light-emitting diode (OLED) microdisplay is its increased electrical and optical crosstalk.⁶ On the other hand, from HDR viewpoint, light leakage from an LCD panel reduces the contrast ratio.^{7,8} To increase contrast ratio and dynamic range, LCDs with dual light modulation layers have been developed. The first light modulation layer is the liquid crystal (LC) panel, and the second layer can be a 2D mini-light-emitting diode (LED) array, a lower resolution density LCD panel, or a laser beam scanning system. Recently, 2D local dimming mini-LED backlights have been rapidly developed to display HDR images for different direct-view displays, such as televisions, tablets, monitors, and automotive displays.^{9–12} For VR applications, mini-LED backlit LCDs are emerging. Some VR products equipped with a mini-LED backlight have been released. However, to mitigate halo artifacts, mini-LED backlight with thousands of local dimming zones is not uncommon; each local dimming zone corresponding to 0.41° viewing angle (i.e., 2.43 zones per degree), when the native LCD contrast ratio is 2000:1.¹¹ With the same local dimming zone density, to achieve 100° field of view (FOV) in a VR headset, we need 243×243 local dimming zones for a 2-in. microdisplay. The corresponding local dimming zone size is only about $150 \mu\text{m}$, which is challenging to fabricate. Therefore, when implementing mini-LED backlit LCDs for VR devices, the density of local dimming zones is often much lower than that of direct-view displays. It is worth noting that FOV stands for the maximum angular size of the object as seen from the entrance pupil. In a VR device, it is the angular size of the virtual image observed by the viewer. Self-emissive displays, such as OLED and micro-LED displays, are regarded as outstanding microdisplay candidates because of their excellent dark state. However, in practical applications, the small pixel size restricts the design of compensation driving circuits, thereby degrading the image quality. Based on the above discussion, for all types of microdisplays, it is extremely difficult to meet the HVS requirements. However, do we really need to design a microdisplay to meet all the demanding HVS requirements remains a good question to be explored.

Although some efforts have been conducted to analyze the image degradation in VR imaging optics^{13–17} and microdisplays⁴ separately, very few has considered both elements together. In this paper, we systematically analyze the image degradation mechanisms of VR devices, and our results indicate that in comparison with microdisplays, the degradation caused by imaging optics such as aberrations and stray light cannot be ignored. Therefore, when we design a microdisplay, we do not have to meet all the requirements of HVS but only need to meet the

requirements of imaging optics. To evaluate the image degradation from imaging optics, we use a ray-tracing simulation model to analyze the point spread function (PSF) of imaging optics. A point source is set up as light emitted from the microdisplay, and its corresponding intensity distribution on the receiver is defined as the PSF of the imaging optics. Therefore, both the aberration and stray light of imaging optics are considered together. However, because we only focus on ray-tracing analysis, diffraction of imaging optics is not considered in this study. Based on our simulation results, by considering the PSF of the imaging optics, we can unleash the contrast and resolution density requirements of the microdisplay while keeping a similar image quality. These results help prevent over-design of microdisplays, such as insane resolution densities of microdisplays and redundant local dimming zones for mini-LED backlights.

2 | PANCAKE LENS DESIGN

As shown in Figure 1A, in this study, for simplicity, we use a single-lens VR imaging optics in the system. Details of the lens design have been reported earlier.^{18,19} The front surface of this pancake lens is a half mirror. The back surface of the pancake lens is a reflective circular polarizer that reflects one circular polarization while transmitting the opposite one. Let us assume it reflects right-handed circularly polarized (RCP) light and transmits the left-handed circularly polarized (LCP) light.

Such a reflective circular polarizer consists of a half-wave ($\lambda/2$) plate, a $\lambda/4$ plate, and a multilayer reflective polarizer. The optical axis of the $\lambda/2$ plate and the $\lambda/4$ plate is at 15° and 75° , respectively, to form a broadband quarter-wave plate. Regarding the reflective polarizer, multilayer films with central wavelengths of 0.42, 0.46, 0.50, 0.55, 0.60, 0.65, 0.70, 0.76, and $0.82 \mu\text{m}$ are used for broadband applications.²⁰ Whereas, more complex optical designs such as two- or three-lens designs and multi-twisted $\lambda/4$ plates²¹ could further improve the PSF and suppress the stray light for the pancake VR devices. However, some of these designs are costly and have alignment issues, and some cause more surface reflections (stray light). The goal of this work is to establish the display requirements based on the optical performance of the VR imaging optics. To keep in mind that different VR imaging optics lead to different display requirements. The measurement system consists of an ideal lens with 4-mm aperture and a receiver located at the focal plane of the ideal lens. When a collimated light impinges the lens at a different angle, it is focused at an off-axis position. Meanwhile, as long as the incident light is not perfectly collimated, the focus on the receiver is blurred.

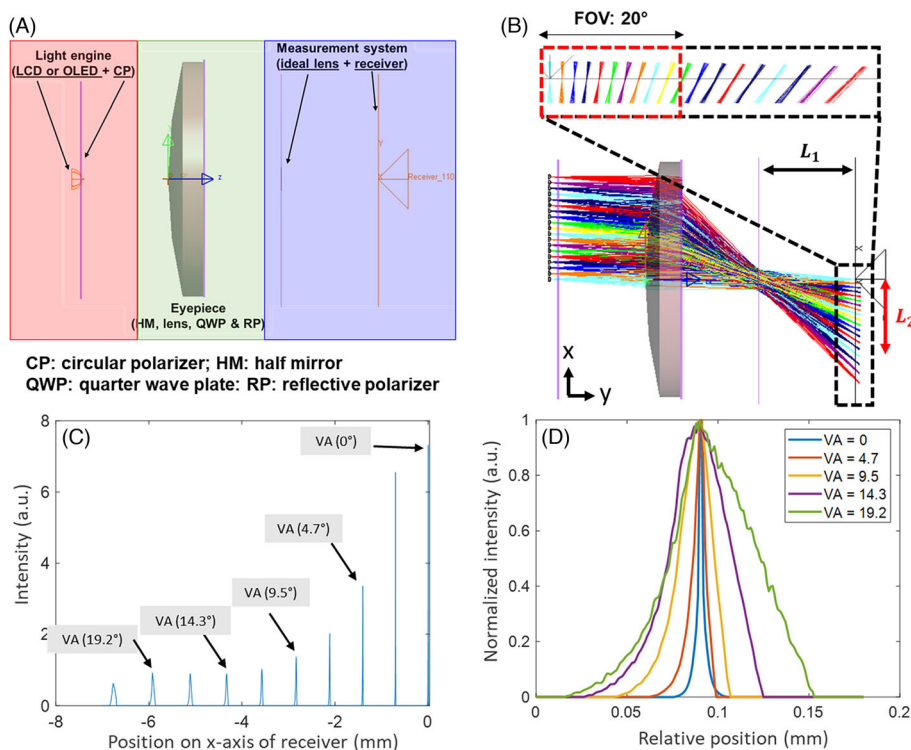


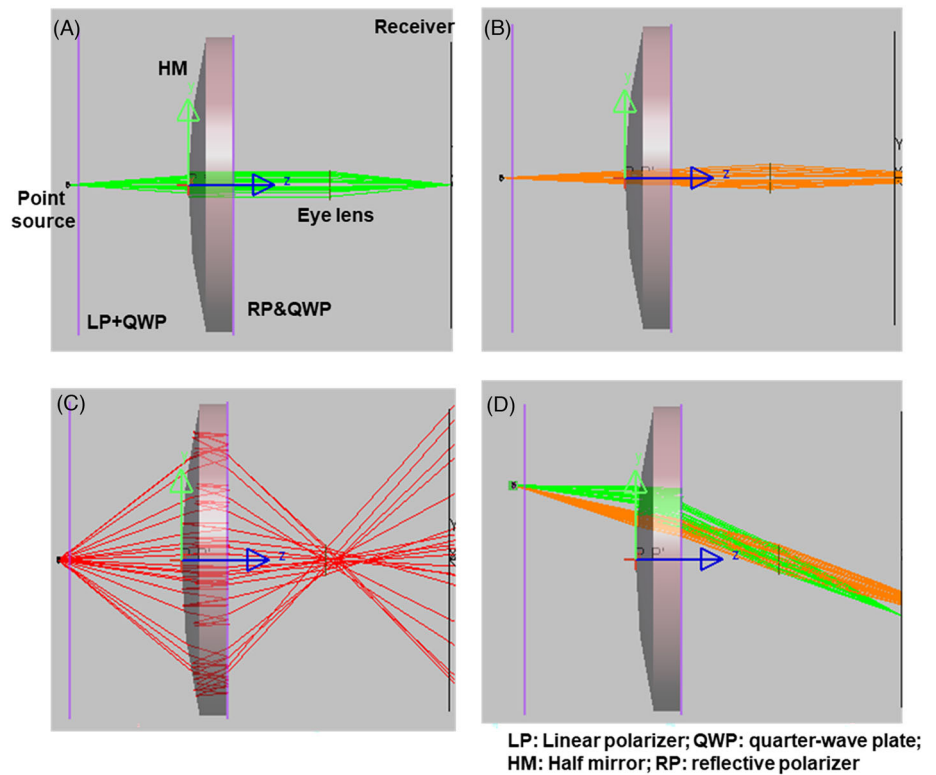
FIGURE 1 (A) Schematic of pancake virtual reality (VR) device in LightTools. (B) The ray path of point source in different positions with 1-mm step. (C) The 1D intensity distribution of each point source. (VA: viewing angle) (D) Normalized intensity distribution of point sources corresponding to different viewing angles, where the peak positions of the different intensity distributions are aligned.

As mentioned above, the PSF of the imaging optics consists of the effects from aberrations and stray light. In this paragraph, let us first focus on the impact of aberrations on image quality; so, we turn off the raytracing of stray light in the optical simulation model. Figure 1B shows the ray paths of point sources at different x-axis positions. The point source at the center corresponds to the normal viewing angle. As the point source moves from the center to the positive x-axis on the microdisplay, the image is formed in the negative x-axis of the receiver. As shown in Figure 1B, the corresponding viewing angle of each point source can be calculated through L_1 and L_2 , where L_1 is the distance between the lens and the receiver and L_2 is the distance between the center of receiver and the imaging point. Different point source corresponds to various L_2 on the receiver and different viewing angle. Figure 1C depicts the intensity distribution of different point source within the 20° FOV, and the corresponding viewing angle is also marked in the figure. Here, we focus on the analysis within 20° FOV, which is a typical eye rotation range. For the FOV larger than 20°, the users often turn their heads. It appears that a point source located far from the center results in a lower peak intensity and a wider spot size. In other words, the resolution of the lens drops sharply. We further align the peak positions of different intensity distributions, as shown in Figure 1D, to illustrate that the intensity distribution broadens with increasing viewing angle. Aberrations widen the intensity distribution, which in turn lowers the maximum resolvable density of

light engines. For a long time, researchers have pursued high-resolution density displays based on the human visual acuity, which is 60 pixels per degree. However, after considering the aberration of VR imaging optics, the target resolution density of light engines should be determined by the resolving power of imaging optics, rather than by the HVS.

In this paragraph, the effect of stray light on the PSF of the imaging optics is considered. Stray light is caused by the surface reflection and depolarization of imaging optics. The optical path scheme of the pancake imaging optics is shown in Figure 2. The non-ideal reflective polarizer and quarter-wave plate cannot convert the light of different wavelength and incident angle to the desired circular polarization as it propagates through the imaging optics. In common practices, the polarization is slightly elliptical, which causes stray light to degrade the image contrast in a VR device. Figure 2A–C shows different types of light paths in different colors: signal (green color), stray light: type 1 (orange color), and stray light: type 2 (red color), respectively. To evaluate the stray light effect, we need to trace the stray light whose intensity is much lower than that of the signal beam. Here, we lower the raytracing power threshold to 10^{-5} , which means rays are traced until the power drops below 10^{-5} . Also, to maintain the simulation accuracy, the total number of traced rays is 2×10^8 , and more importantly, after a ray hits each surface, it is further split into reflected, transmitted, and absorbed rays. Compared to the signal beam passing through the pancake lens three times, type 1 stray

FIGURE 2 The scheme demonstrating the light path for a pancake virtual reality (VR) device. The path of (A) signal ray (green color), (B) stray light (type 1; orange color), and (C) stray light (type 2; red color) in the LightTools simulation model. (D) The path of signal ray (green color) and stray light (type 1; orange color) of an off axis point source.



light passes through the pancake lens only once. Therefore, it has a shorter optical path in the pancake lens, that is, it experiences a smaller optical power. This insufficient lens power results in a diverging beam impinging on the ideal lens, and the diverging beam would be focused farther from the intended receiver. By contrast, type-2 stray light is reflected twice by the reflective polarizer (RP) and experiences a stronger lens power than the signal beam. As a result, the ray path is focused in front of the intended receiver. Additionally, Figure 2D illustrates the stray light from an off axis point source, where the center of the stray light is separated from the signal beam. In other words, ghost images caused by stray light do not surround the target image point but are separated from it. It is worth mentioning that in Figure 2D we only show the signal beam and type 1 stray light, which are the ray paths with maximum power, without including the type 2 stray light, to keep the figure visible. For the point source located at the center of display, the power ratio of stray light to signal ray is about 3.65%. This value is comparable to the result (2%–10%) reported in the paper of Hou et al.²²

After separately introducing the effects of aberrations and stray light on the PSF of the imaging optics, we take both factors into consideration in the following analysis. Different test patterns as shown in Figure 3A are applied to the VR device to evaluate the stray light effect on image contrast. The white image size corresponds to a FOV of approximately 40° ($\pm 20^\circ$). In each test pattern,

the central black image occupies 2.5, 7, and 12° of FOV, respectively. For an ideal imaging optics, the central area should be black (intensity = 0). However, the stray light from adjacent pixels lowers the image contrast, as Figure 3B–D shows. Here, the image contrast is defined by the ratio of average intensity of dark areas to the average intensity of bright areas. The image contrast for the three presented patterns is 108:1 (FOV = 2.5°), 236:1 (FOV = 7°), and 422:1 (FOV = 12°), respectively. Figure 3 illustrates that although a perfect microdisplay is applied, the image contrast is severely degraded by the stray light of imaging optics. It is worth mentioning that when the dark area expands to about 12° FOV, the intensity at the center of the dark area is reduced to zero. As a result, we did not continue to increase the dark area size.

3 | MICRODISPLAYS

From the perspective of microdisplays, two types of microdisplays are widely used in VR headsets: LCDs and OLED displays. Because of the limited intrinsic contrast of LCDs (<5000:1), the small light leakage in the dark state cause image artifacts in a VR device. In the following, we evaluate the dark state of a display with a contrast ratio of 500:1, 1000:1, 2000:1, and 10^6 :1 (perfect dark state). Here, OLEDs, mini-LED backlit LCDs, and micro-LEDs are considered as having a perfect dark state, where

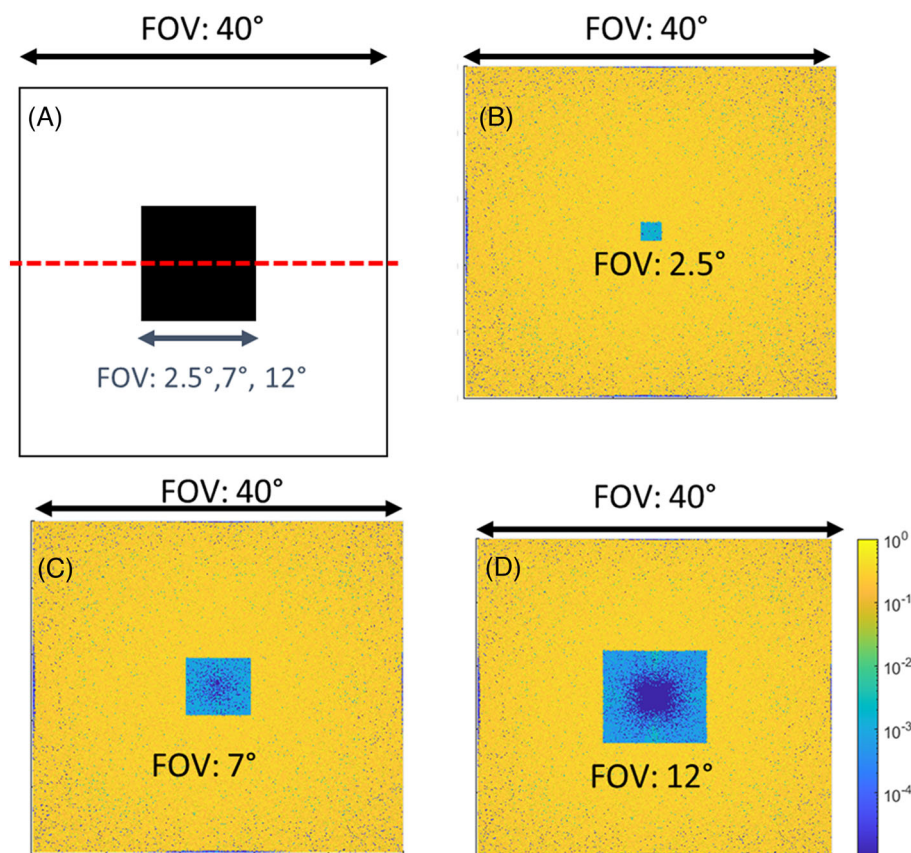


FIGURE 3 (A) The test pattern with different size of dark region (field of view [FOV] = 2.5, 7 and 12°). Normalized intensity distributions of test patterns with dark regions corresponding to (B) 2.5, (C) 7, and 12° FOV.

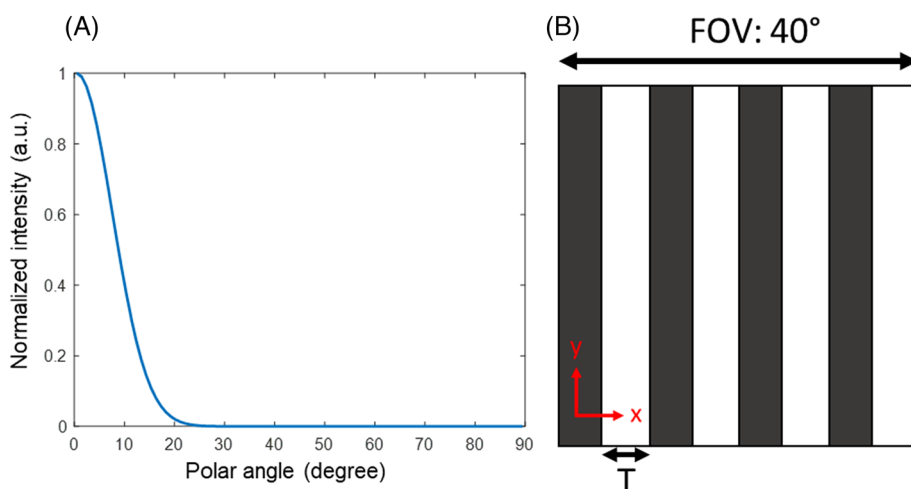


FIGURE 4 (A) Directional radiation pattern of the microdisplay. (B) Test pattern with various resolution density: $T = 500, 200, 100, 40,$ and $20 \mu\text{m}$, and the size corresponding to 40° field of view (FOV).

the brightness of dark state is zero. The radiation pattern of the display is set to be directional as Figure 4A shows.

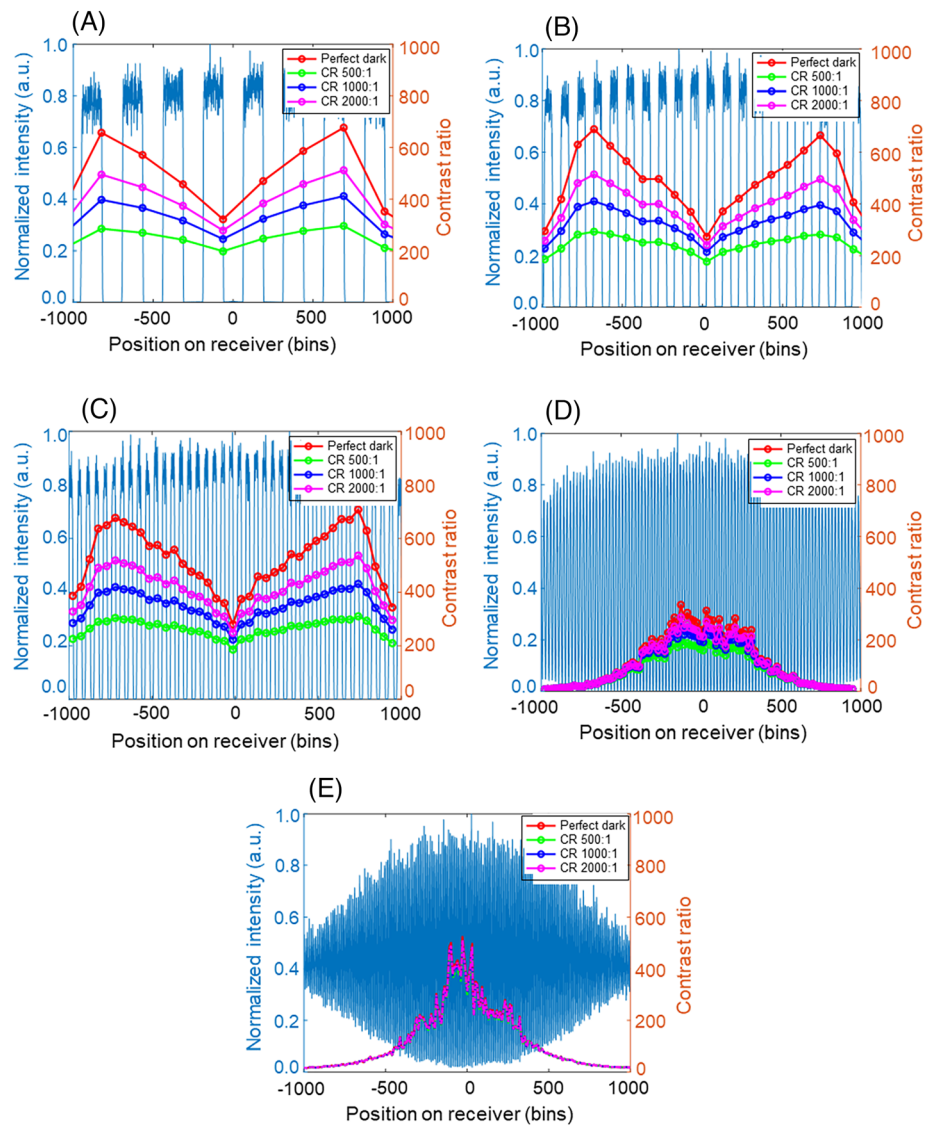
Moreover, to evaluate the image quality of a VR device, the test patterns with frequency of [0.38, 0.95, 1.9, 4.75, and 9.5] cycles per degree (cpd) is displayed by the microdisplay. The corresponding line width (T) of each resolution pattern on the display is 500, 200, 100, 40, and $20 \mu\text{m}$, respectively, and the pattern size is 40° FOV as Figure 4B depicts. To support a $20\text{-}\mu\text{m}$ line width, the resolution density of the microdisplay should be higher than 1270 ppi.

4 | RESULTS AND DISCUSSION

Figures 5 and 6 illustrate the intensity distribution on the receiver for different test patterns analyzed by the optical model shown in Figure 1A. Because the test pattern only varies along x-axis but remains uniform along y-axis (Figure 4B), the intensity distribution is averaged along y-axis.

We plot the average intensity distributions on linear and logarithmic scales in Figures 5 and 6, respectively. Logarithmic scale images help illustrate the intensity

FIGURE 5 Intensity distributions in linear scales of test patterns with resolutions of (A) 0.38, (B) 0.95, (C) 1.9, (D) 4.75, and (E) 9.5 cpd. The corresponding contrast ratio distributions of microdisplays with various contrast ratios are also plotted.



distribution at low intensity levels. Therefore, the effects of stray light are more easily observed. Figure 5A–E corresponds to different pattern frequencies. Additionally, the bin ranges on the receiver are -1000 bins and 1000 bins, corresponding to the viewing angle ranges of -10° and $+10^\circ$. In another word, 2000 bins correspond to a FOV of 20° (one bin: 0.01°). Let us first focus on the results for a perfect dark-state panel (e.g., OLED or micro-LED) whose image degradation is caused only by the imaging optics. For the low frequency test patterns (0.38, 0.95 and 1.9 cpd), the pattern remains clear over the entire receiver area. The image contrast degradation is mainly caused by the stray light from the imaging optics. In these figures, the dark state ranges from 0.001 to 0.003, depending on the location. To clearly demonstrate the dark-state variation, Figure 6A–E depicts the average intensity distribution on the receiver in a logarithmic scale. This stray light sets the upper limit for the

device contrast ratio to about a few hundreds to one, even when the dark state of display is set to be completely black. The contrast variation is mainly determined by the stray light distribution on the receiver. As the test pattern frequency increases (4.75 and 9.5 cpd), the patterns from large viewing angles are merged so that the image contrast decreases. Therefore, image contrast gradually decreases with increasing viewing angle. The maximum image contrast in the center view is about 300:1 (4.75 cpd) and 50:1 (9.5 cpd). Under the high-frequency pattern, we notice that the image contrast is mainly determined by the aberration of the imaging optics. At larger viewing angles, the widened PSF caused by aberration severely reduces the image contrast. Under such condition, the stray light no longer makes a significant impact on the image contrast. Overall, for low-frequency target images, the image quality is mainly affected by the stray light from the imaging optics. By contrast,

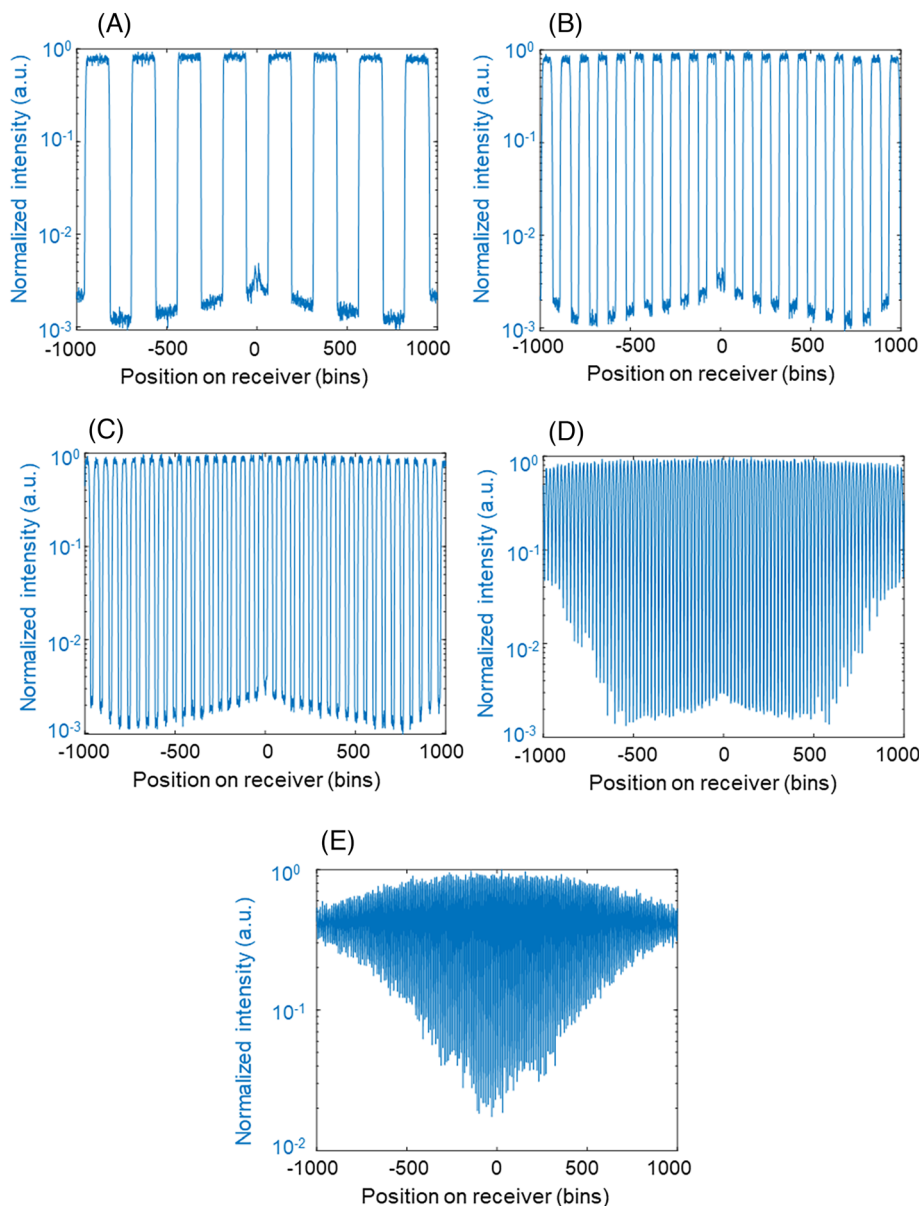


FIGURE 6 Intensity distributions in logarithmic scales of test patterns with resolutions of (A) 0.38, (B) 0.95, (C) 1.9, (D) 4.75, and (E) 9.5 cpd.

for high-frequency target images, the image quality is mainly degraded by the aberration of the imaging optics.

Display artifacts, such as light leakage from the LCD, are also considered in the simulation. Figure 6A–C illustrates that the light leakage from LCD is comparable to (or even weaker than) the intensity of stray light (0.001 to 0.003). Therefore, compared to an OLED display with a perfect dark state, as shown in Figure 5A–C, the imperfect display contrast only reduces the peak image contrast by [43%, 60%, and 80%] for an LCD with CR = [500:1, 1,000:1, 2000:1], respectively. Moreover, boosting display contrast by 4 \times , for example, from 500:1 to 2000:1, only improves the image contrast by 1.8 \times . In other words, due to the disturbance of stray light, simply increasing the display contrast cannot achieve the expected high-contrast image, that is, the benefit of increasing display

contrast is limited. For high-resolution patterns, the image contrast degrades severely because the aberration leads to pattern merging as shown in Figure 6D,E. Under this condition, display artifacts do not cause a significant reduction in image contrast. Additionally, the aberration of the imaging optics limits the maximum resolvable density of light engines to \sim 9.5 cpd, which corresponds to 1270 ppi for the microdisplay. Therefore, the benefit to further increase the display's resolution density is not obvious in our pancake VR device. It is worth noting that the optical resolving power of the VR imaging optics depends on the lens design. Some two-lens or three-lens designs may offer a higher optical resolving power and thus shall require a higher resolution density display.

Recently, using mini-LED backlight to achieve HDR for LCDs has attracted much attention. However, how to

design the number of local dimming zones remains unclear. Here, based on the above analysis, we plot the image contrast under normal view as a function of pattern frequency, as shown in Figure 7. Notably, the lowest pattern frequency is as low as 0.0475 cpd. Same as the above analysis, for high-frequency patterns (>5 cpd), the aberration of the VR device is the dominant factor affecting the image contrast. Regardless of the display performance, the image contrast is almost the same because the aberration of the VR device results in pattern merging. For the frequency ranging from 0.1 cpd to 5 cpd, stray light is a major contributor to the decreased image contrast and there is no noticeable gain in increasing the display contrast. For low-frequency patterns (<0.1 cpd), the intrinsic contrast of the microdisplay becomes the dominant factor affecting the image contrast. A high contrast microdisplay significantly improves the image contrast of a VR device. From a mini-LED backlight design perspective, the smaller local dimming zone size support a higher frequency pattern with a higher display contrast. On the other hand, a larger local dimming zone size only support lower frequency modes with a high display contrast. Based on above discussion, it is not helpful to apply extremely small-sized local dimming zones to support high-frequency test patterns with a high display contrast. This is because the image contrast of a VR device for high-frequency image contents is primarily determined by the optical properties of the imaging optics (stray light and aberration of imaging optics). A high display contrast helps improve the VR image contrast when the pattern

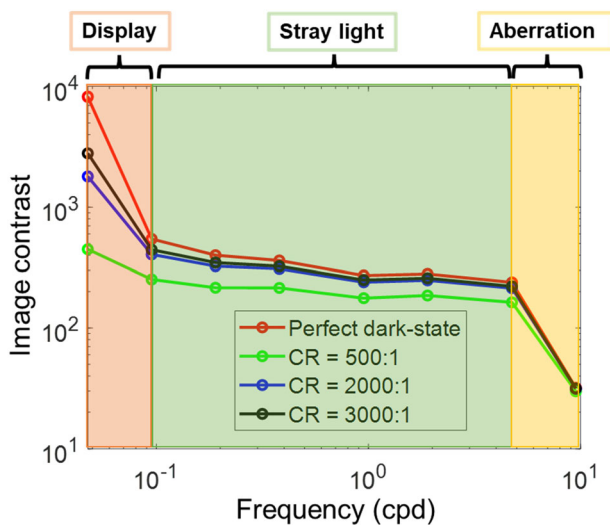


FIGURE 7 Simulated image contrast of a virtual reality (VR) device of test pattern with different frequency (0.0475 to 9.5 cycles per degree [cpd]). Aberrations, stray light, and display contrast mainly determine the image contrast for high-frequency (>5 cpd), mid-frequency (>0.1 and <5 cpd), and low-frequency (<0.1 cpd) image content, respectively.

frequency is low. As Figure 7 shows, when the test pattern frequency is between 0.1 and 0.0475 cpd (pink region), a higher display contrast ratio makes a more noticeable contribution to the VR image contrast. The 0.1- and 0.0475-cpd test pattern frequency corresponds to 2 and 4-mm width in the microdisplay, respectively. Therefore, considering a 40-mm \times 40-mm microdisplay supporting a 100° FOV, the desired local dimming zone number is about 400 (20 \times 20) to 100 (10 \times 10), depending on the intrinsic LCD contrast. For an LCD with $CR \geq 2000:1$, the image contrast is comparable to an OLED display with a perfect dark state, even with test patterns frequencies as low as 0.1 cpd. Therefore, we only require about 100 (10 \times 10) local dimming zones to see a significantly improved image contrast when the frequency is below 0.1 cpd. On the other hand, for an LCD with $CR = 500:1$, the image contrast at a frequency of 0.1 cpd is noticeably different from that of an OLED display. Thus, about 400 (20 \times 20) local dimming zones would be required to improve the image contrast of test pattern with 0.1-cpd frequency. This value is close to that of commercial product such as Meta Quest Pro, which has about 500 mini-LED local dimming zones.

Further subjective experiments or human visual models, which take the contrast sensitivity function of HVS into consideration, are essential to determine the indistinguishable image contrast difference. In the above simulation, the test pattern has an average picture level (APL) of 50% (half the pixels on and half off) and a size range of 40° FOV. In practice, the severity of stray light depends on the APL of the image content. When more pixels are turned on, the adjacent pixels receive more stray light, which in turn reduces the image contrast. Moreover, the birefringence of the lens is not considered in our simulations.²³ Therefore, further comparisons between the simulation results and physical experimental results are necessary.

5 | CONCLUSION

Through systematic analysis of the image defects in a pancake VR device caused by both imaging optics and microdisplay, we define the requirements for the microdisplays. The image contrast of fringe patterns at different frequencies is used as an evaluation metrics. In our VR imaging optics, the aberration of the imaging optics limits the maximum resolvable density of light engines, and the stray light of imaging optics, although undesirable, sets the upper limit for the device contrast ratio. Furthermore, enhancing the display contrast only significantly improves the image contrast of low-frequency contents (<0.1 cpd). Therefore, when applying local

dimming technology to LCD microdisplays, the size of the local dimming zone does not need to be very small. It just needs to be properly sized (around 2- to 4-mm wide, depending on the intrinsic LCD's contrast ratio) to improve the image contrast of low-frequency patterns. Overall, based on our systematic analysis, the specific requirements of microdisplays are defined in terms of cooperative imaging optics.

ACKNOWLEDGMENTS

The UCF group is indebted to Nichia Corporation for the financial support and Hajime Akimoto for stimulating discussion.

ORCID

Zhiyong Yang  <https://orcid.org/0000-0002-7181-7443>

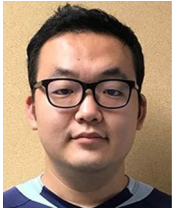
Shin-Tson Wu  <https://orcid.org/0000-0002-0943-0440>

REFERENCES

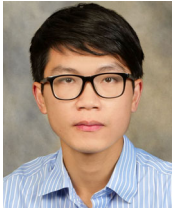
- Xiong J, Hsiang EL, He Z, Zhan T, Wu ST. Augmented reality and virtual reality displays: emerging technologies and future perspectives. *Light Sci Appl*. 2021;10(1):216. <https://doi.org/10.1038/s41377-021-00658-8>
- Steinicke F. *Being really virtual. Immersive natives and the future of virtual reality*: Springer; 2016. <https://doi.org/10.1007/978-3-319-43078-2>
- Kress BC, Peroz C. Optical architectures for displays and sensing in augmented, virtual, and mixed reality (AR, VR, MR). *Proc SPIE*. 2020;11310:1131001.
- Vieri C, Lee G, Balram N, Jung SH, Yang JY, Yoon SY, et al. An 18 megapixel 4.3 "1443 ppi 120 Hz OLED display for wide field of view high acuity head mounted displays. *J Soc Inf Disp*. 2018;26(5):314–24. <https://doi.org/10.1002/jsid.658>
- Hsiang EL, Yang Z, Yang Q, Lai PC, Lin CL, Wu ST. AR/VR light engines: perspectives and challenges. *Adv Opt Photonics*. 2022;14(4):783–861. <https://doi.org/10.1364/AOP.468066>
- Penninck L, Diethelm M, Altazin S, Hiestand R, Kirsch C, Ruhstaller B. Modelling crosstalk through common semiconductor layers in AMOLED displays. *J Soc Inf Disp*. 2018;26(9):546–54. <https://doi.org/10.1002/jsid.671>
- Yoneya M, Utsumi Y, Umeda Y. Depolarized light scattering from liquid crystals as a factor for black level light leakage in liquid-crystal displays. *J Appl Phys*. 2005;98(1):016106. <https://doi.org/10.1063/1.1948524>
- Chen H, Tan G, Li MC, Lee SL, Wu ST. Depolarization effect in liquid crystal displays. *Opt Express*. 2017;25(10):11315–28. <https://doi.org/10.1364/OE.25.011315>
- Chen E, Guo J, Jiang Z, Shen Q, Ye Y, Xu S, et al. Edge/direct-lit hybrid mini-LED backlight with U-grooved light guiding plates for local dimming. *Opt Express*. 2021;29(8):12179–94. <https://doi.org/10.1364/OE.421346>
- Masuda T, Watanabe H, Kyoukane Y, Yasunaga H, Miyata H, Yashiki M, et al. 28-3: mini-LED backlight for HDR compatible mobile displays. *SID Symp Dig Tech Pap*. 2019;50(1):390–3. <https://doi.org/10.1002/sdtp.12939>
- Tan G, Huang Y, Li MC, Lee SL, Wu ST. High dynamic range liquid crystal displays with a mini-LED backlight. *Opt Express*. 2018;26(13):16572–84. <https://doi.org/10.1364/OE.26.016572>
- Hsiang EL, Yang Q, He Z, Zou J, Wu ST. Halo effect in high-dynamic-range mini-LED backlit LCDs. *Opt Express*. 2020;28(24):36822–37. <https://doi.org/10.1364/OE.413133>
- Geng Y, Gollier J, Wheelwright B, Peng F, Sulai Y, Lewis B, et al. Viewing optics for immersive near-eye displays: pupil swim/size and weight/stray light. *Proc SPIE*. 2018;10676:19–35.
- Peng F, Geng Y, Wang J, Lu L, Zhao Y, Maimone A, et al. 33-1: invited paper: liquid crystals for virtual reality (VR). *SID Symp Dig Tech Pap*. 2021;52(1):427–30. <https://doi.org/10.1002/sdtp.14708>
- Huxford RB. Wide FOV head-mounted display using hybrid optics. *Proc SPIE*. 2004;5249(1):230–7.
- Narasimhan BA. Ultra-compact pancake optics based on thin eyes super-resolution technology for virtual reality headsets. *Proc SPIE*. 2018;10676:359–66.
- Cheng D, Hou Q, Li Y, Zhang T, Li D, Huang Y, et al. Optical design and pupil swim analysis of a compact, large EPD and immersive VR head mounted display. *Opt Express*. 2022;30(5):6584–602. <https://doi.org/10.1364/OE.452747>
- LaRussa JA, Gill AT. The holographic pancake window TM. *Proc SPIE*. 1978;0162:120–9.
- Zou J, Zhan T, Hsiang EL, Du X, Yu X, Li K, et al. Doubling the optical efficiency of VR systems with a directional backlight and a diffractive deflection film. *Opt Express*. 2021;29(13):20673–86. <https://doi.org/10.1364/OE.430920>
- Li Y, Wu TX, Wu ST. Design optimization of reflective polarizers for LCD backlight recycling. *J Disp Technol*. 2009;5(8):335–40. <https://doi.org/10.1109/JDT.2009.2027033>
- Li L, Escuti MJ. Super achromatic wide-angle quarter-wave plates using multi-twist retarders. *Opt Express*. 2021;29(5):7464–78. <https://doi.org/10.1364/OE.418197>
- Hou Q, Cheng D, Li Y, Zhang T, Li D, Huang Y, et al. Stray light analysis and suppression method of a pancake virtual reality head-mounted display. *Opt Express*. 2022;30(25):44918–32. <https://doi.org/10.1364/OE.476078>
- Maiti SN, Saroop UK, Misra A. Studies on polyblends of poly(vinyl chloride) and acrylonitrile-butadiene-styrene terpolymer. *Polym Eng Sci*. 1992;32(1):27–35. <https://doi.org/10.1002/pen.760320106>

How to cite this article: Hsiang E-L, Yang Z, Wu S-T. Optimizing microdisplay requirements for pancake VR applications. *J Soc Inf Display*. 2023; 31(5):264–73. <https://doi.org/10.1002/jsid.1199>

AUTHOR BIOGRAPHIES



En-Lin Hsiang received his BS degree from National Chiao Tung University, Hsinchu, Taiwan in 2014 and MS degree from National Chiao Tung University, Hsinchu, Taiwan, in 2016. Currently, he is working toward having a PhD degree at College of Optics and Photonics, University of Central Florida, USA. His current research focuses on mini-LED backlight, OLED, and micro-LED for flat panel displays and light engines for AR/VR display systems.



Zhiyong Yang received his BS degree in Optoelectronic Engineering from Chongqing University in 2017 and MS degree in Optics & Photonic from the University of Michigan in 2019. Currently, he is working toward a PhD degree from the College of Optics and Photonics, University of Central

Florida. His current research interests include liquid-crystal-on-silicon, mini-LED backlight, OLED display, and micro-LED display.



Shin-Tson Wu is a Trustee Chair professor at the College of Optics and Photonics, University of Central Florida (UCF). He is an Academician of Academia Sinica, a Charter Fellow of the National Academy of Inventors, and a Fellow of the IEEE, OSA, SID, and SPIE. He is a recipient of the Optica Edwin H. Land Medal (2022), SPIE Maria Goeppert-Mayer Award (2022), Optica Esther Hoffman Beller Medal (2014), SID Slottow-Owaki Prize (2011), Optica Joseph Fraunhofer Award (2010), SPIE G. G. Stokes Award (2008), and SID Jan Rajchman Prize (2008). In the past, he served as the founding Editor-In-Chief of the Journal of Display Technology, Optica publications council chair and board member, and SID honors and awards committee chair.